Clean Transfer of Graphene for Isolation and Suspension

Yung-Chang Lin,[†] Chuanhong Jin,[‡] Jung-Chi Lee,[†] Shou-Feng Jen,[†] Kazu Suenaga,[‡] and Po-Wen Chiu[†,*]

[†]Department of Electrical Engineering, National Tsing Hua University, Hsinchu 30013, Taiwan, and [‡]National Institute of Advanced Industrial Science and Technology (AIST), Tsukuba 305-8565, Japan

ABSTRACT Fabrication of large-area clean graphene sheets is the first step toward the development of high-performance applications in surface chemistry and biotechnology as well as in high-mobility electronics. Here we demonstrate the clean transfer of graphene grown by chemical vapor deposition on Cu foil, with surface cleanness defined by transmission electron microscopy (TEM) in combination with Raman scattering on the same position of suspended graphene sheets. For clean graphene, the Raman spectra exhibit distinctive features that can explicitly discriminate from that of graphene covered with a thin layer of amorphous carbon such as residual poly(methyl methacrylate) (PMMA). By applying this technique to graphene sheets with various degrees of surface cleanness, we show that the quantitative characterization of the thickness of surface contaminants is possible based on multiple reflections and interference of light in samples.

KEYWORDS: graphene · suspension · isolation · PMMA · clean transfer

Graphene is a single atomic layer of carbon constructed in an sp^2 honeycomb lattice, with each individual atom exposed to an external environment that decisively determines its physical and chemical properties.[1] Existing graphene gas sensors make use of this property for highly sensitive gas detection.[2] Surface chemistry that brings external molecules into direct reaction with graphene requires the sheet to be free of contaminants so that the desired chemical reaction can occur homogeneously. As a result, extra-clean large-area graphene sheets may provide a playground for molecular imaging on periodic graphene lattice under transmission electron microscopy (TEM)[3−5] and for improving the efficiency of DNA sequencing,[6] drug delivery,[7] or molecular doping[8,9] for device applications. However, large-area graphene sheets often need to be isolated from their growing substrate and then transferred to the target materials or mechanical supports with the aid of poly(methyl methacrylate) (PMMA).[10] PMMA's easy handling and processing, as well as its variable viscosity, make it ideal for assisting graphene transfer, but at the cost of surface contamination due to the strong dipole interactions between PMMA and chemical groups on graphene. This results in a thin layer of residual long-chain molecules sticking to the graphene even after an exhaustive rinse with organic solvents such as acetone or 1-methyl-2-pyrrolidone. It was recently shown by Aleman *et al.* that clean graphene membranes can be obtained in a transfer-free process where graphene was suspended directly on the growing Cu foils.[11] Patterned Cu foils act as scaffolds to provide sufficient mechanical supports and can be scaled up for a wafer-size production.

Here we present a systematic work on graphene transfer and suspension that uses poly(bisphenol A carbonate) (PC) as the supporting material. Our strategy is motivated by recent experimental work that replaces PMMA with PC for graphene suspension.[12] PC can be easily removed by organic solvents without the need of further annealing in the forming gas, thus making clean transfer feasible. To characterize the transferred graphene, a sophisticated but clean lithography technique is also developed so that the free-standing graphene can be confined by distinguishable markers and the surface cleanness can be, therefore, examined by high-resolution TEM in atomic scale in combination with Raman measurements in the proximity of the same location. To establish a quantitative characterization of the surface cleanness based on Raman scattering, we use the conventional PMMA transfer technique and anneal the resulting graphene to different degrees of cleanness. We show that surface cleanness of suspended graphene can be simply defined by means of the relative intensity of the characteristic Raman G mode. Different coverage of the residual PMMA, revealed by TEM, causes distinctive Raman spectra due to the different conditions for the multiple reflections and interference of light between the contaminants and graphene.

* Address correspondence to pwchiu@ee.nthu.edu.tw.

Received for review January 11, 2011 and accepted February 16, 2011.

Published online February 25, 2011
10.1021/nn200105j

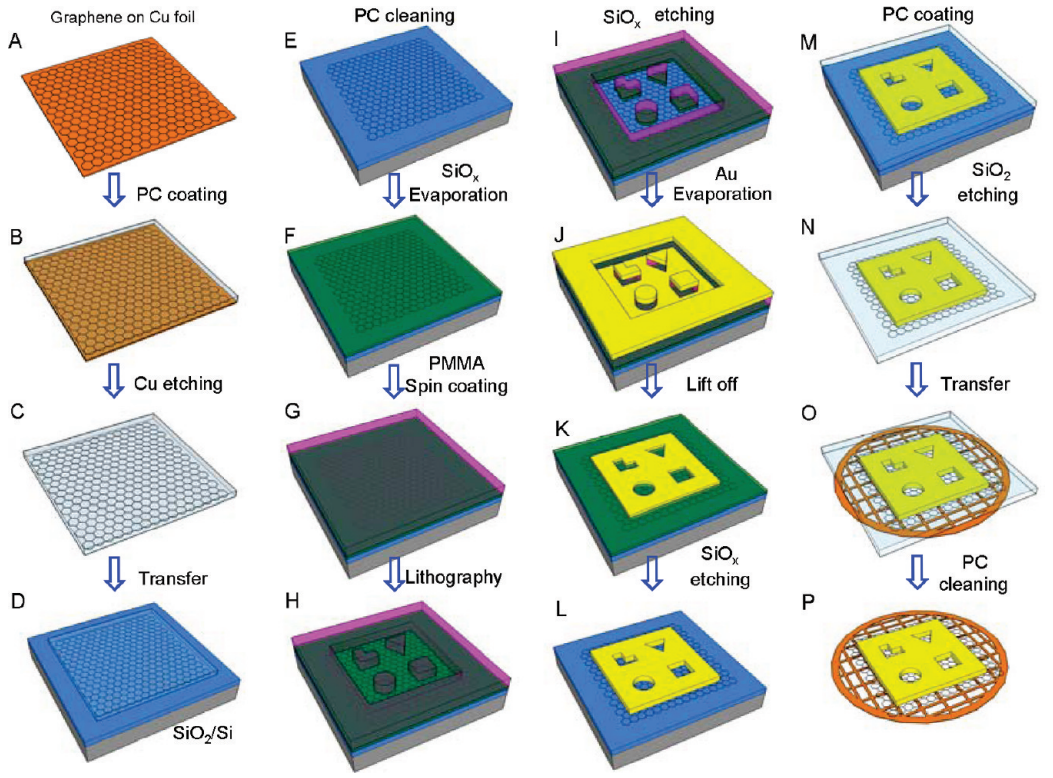

Figure 1. Process flow of clean graphene transfer from metal to silicon substrate using polycarbonate film as support (steps A—E) and subsequent lithographic patterning for free-standing graphene on Au patterns (step F—P).

RESULTS AND DISCUSSION

Figure 1 schematically illustrates the processes of clean transfer (steps A—E) and subsequent lithographic patterning (steps F—P). The graphene sheets used in the current study were grown by chemical vapor deposition (CVD) on Cu foil.[13] The self-limiting growth mechanism results in over 80% of single-layer graphene coverage. To produce suspended structures, graphene sheets were coated with a PC ~1.5 μm in thickness, followed by etching in ferric chloride (0.03 g/mL) aqueous solution to remove the Cu foil. The resulting PC film with the attached graphene was then transferred onto a silicon substrate. The PC layer can be completely removed with chloroform. A thin layer of nonstoichiometric SiO_x was then evaporated onto the graphene as a protecting layer, followed by a spin coating of PMMA. The SiO_x film prevents the graphene from coming into direct contact with the PMMA. Using standard e-beam lithography, the desired patterns were created and the SiO_x layer was etched by buffered HF solution prior to the metal evaporation (100 nm Au). Again by using PC, the Au/graphene film was separated from the silicon substrate by immersing the whole structure in buffered HF solution. After transferring the Au/graphene film onto a 300-mesh TEM grid, critical point drying was applied to avoid damage to the graphene. The technique described above provided a clean graphene surface for high-resolution TEM imaging and, importantly, is capable of combining TEM with Raman and transport characterizations at the same position on the graphene sheet.

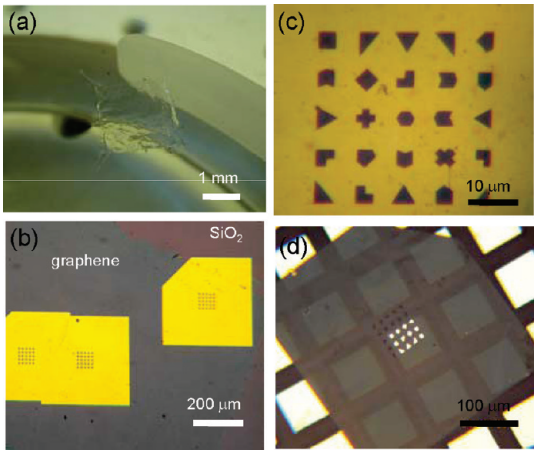

Figure 2. (a) Optical photograph of a suspended graphene/PC film on pure water following the removal of Cu foil (step C in Figure 1). (b) Graphene on Si substrate with Au patterns on top (step I in Figure 1). (c) Au hollow patterns for combining TEM and Raman measurements on graphene. (d) Suspended Au/graphene film on a TEM grid.

Figure 2 shows part of the optical photographs in the transfer processes. Different concentrations of PC in chloroform solution were prepared to fine-tune the viscosity of the PC film on the graphene/Cu foil. The current study used 1.2 wt % of PC solution. In some cases, benzene can be of help in controlling the volatility of the chloroform solvent and prevent

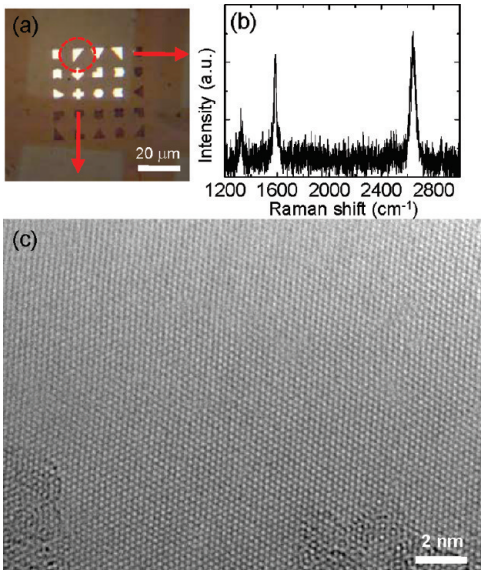

Figure 3. (a) Suspended Au/graphene film on a TEM grid, obtained by PC transfer process. (b) Raman spectrum of graphene, taken at the position indicated by the dotted circle. (c) Corresponding TEM image of graphene in (b).

damage to the graphene, but special care needs to be taken, such as the last step depicted in Figure 1. Rapid dissolution of the PC film in the pure chloroform may fatally disrupt the graphene sheet or cause tears. A gradual transition from different concentrations of acetone-buffered chloroform was thus used to avoid possible damage to the graphene during the transfer. The process described above is superior to the method that uses PMMA as support in that a large clean area can be obtained without the need for annealing.

Figure 3 shows an optical photograph of the device suspended on a TEM grid, together with the Raman spectrum and TEM image in the proximity of the same position on the graphene sheet. The three most intense Raman peaks are located at 1324, 1585, and 2643 cm^{-1}, respectively, representing D, G, and 2D modes.[14,15] The G peak stems from the E_{2g} in-plane optical vibrational mode at the Brillouin zone center. The peak position offers a good estimation of the charge density in graphene,[16,17] while the line width (full width at half-maximum, γ) is a measure of the strength of the electron−phonon coupling.[18,19] For clean suspended graphene, as in this case, the Fermi level lies close to the charge neutrality point for which the G peak position is ~1584 cm^{-1}.[18] A weak p-doping is expected in our case due to the charge transfer from the contact metal.[20] The γ_G was found to reduce from 30 cm^{-1} on the Cu substrate to 16 cm^{-1} in the suspended state, indicating a decrease of electron−phonon coupling strength following suspension.[19] Another significant feature here is the D peak, which responds to the TO phonons around the **K** point of the Brillouin zone and is activated by defect-induced double resonance scattering.[21] The observed D peak in Figure 3b is attributed in part to defects generated during the etching of the Cu substrate and in part to the bulge structures overgrown on the graphene. These structures are hard to remove even after annealing and may be responsible for the low charge mobility in CVD graphene. It is worth noting that the Raman spectrum shown in Figure 3b exhibits a very high noise level and low peak intensities. In fact, these features are related to the graphene surface state and reflect the degree of cleanness, which is negatively correlated with the Raman intensity, due mostly to the lack of multiple light reflections from the clean single-layer graphene sheet, which is discussed below in detail.

To provide insight into the correlation between the surface state and Raman information, graphene transferred by PMMA was also used. Three different degrees of surface cleanness were obtained from different conditions of thermal annealing. Figure 4 compares the TEM images and corresponding Raman spectra acquired with the same integration time for the three suspended graphene sheets. The use of PMMA as transfer support or as e-beam resist for lithography is known to leave a thin layer of residual PMMA on the graphene or carbon nanotubes even after an intensive rinse with various organic solvents.[22] This amorphous PMMA masks the observation of the graphene's atomic structure (Figure 4a). As seen in the TEM image in Figure 4b, thermal annealing between 200 and 250 °C in forming gas helps remove part of the contamination.[23] Small clean spots can be found occasionally in local areas. Prolonged annealing is of little help in this case, while alternate annealing under hydrogen and oxygen atmospheres was found to be more effective in cleaning up the residual PMMA, although it is time-consuming and may cause damage or lattice defects in suspended graphene. Figure 4c shows the TEM image of graphene after such annealing. The two tears indicated by the red arrows were intentionally created by focused electron beam irradiation so as to identify the number of graphene layers. The clean area on the graphene can be enlarged to 100−200 nm, and the contaminants were found to be continuously distributed in the form of networks. Some of the nonperiodic (bulge) structures are due to the nature of the CVD-grown graphene and are hard to distinguish from external contaminants.

Combining TEM with Raman characterizations, we can explicitly evaluate the Raman spectra of the graphene sheets with more defined surface states (Figure 4d−f). Three distinctive features can be seen in the Raman spectra of the suspended clean graphene: (a) a relatively low signal-to-noise ratio; (b) low absolute Raman intensity; and (c) absence of low-frequency (1100−1600 cm^{-1}) broad background. For clean graphene, the lack of multiple reflections of incident light results in a high noise level and low intensity in the Raman signals,[24−27] as shown in

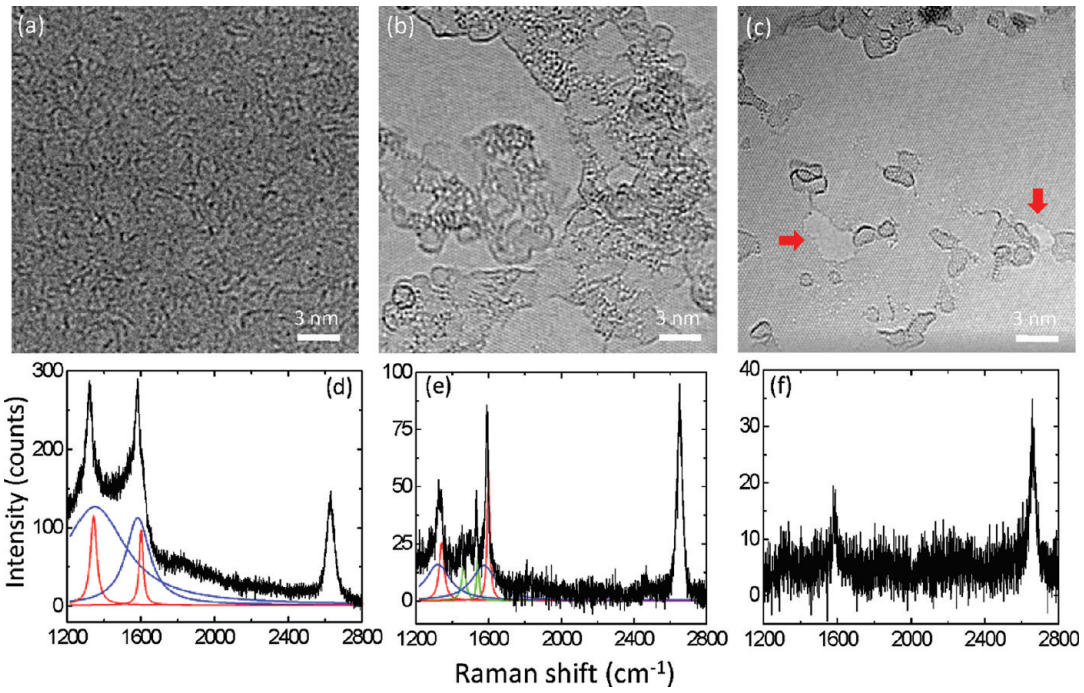

Figure 4. (a) TEM image of graphene fully covered with residual PMMA following free-standing. (b) TEM image of graphene partially covered with residual PMMA after annealing under hydrogen atmosphere. (c) TEM image of clean graphene after annealing under alternate hydrogen and oxygen atmospheres. (d−f) Corresponding Raman spectra of graphene shown in (a−c), respectively. The two sharp red peaks are the fits to the Raman G and D modes of graphene, while the two blue broad peaks are the fits for the Raman G and D modes of amorphous carbon. Two additional green peaks, centered at 1450 and 1530 cm^{-1}, appear in (e) due to the densification of the residual PMMA after annealing.

Figure 4f. This property, in fact, offers means of quickly inspecting surface cleanness. The noise level for clean graphene (Figure 4f) is found to be about 3 times higher than that for partially clean graphene (Figure 4e) and 5 times higher than that for graphene covered with ~2 nm of PMMA (Figure 4d). For unclean graphene (Figure 4d,e), two prominent features can be seen: high absolute Raman intensity and remarked low-frequency signals superimposed on the sharp G and D peaks. This broad signal spans from 1100 to 1600 cm^{-1}, indicative of the existence of amorphous carbon (mixture of sp^2- and sp^3-bonded carbon) due to the residual PMMA.[28,29] The spectrum in this range can be deconvoluted into four components: the two distinct peaks (red fits) are assigned to the G and D modes of graphene,[28] while the other two broad peaks (blue fits) at similar positions originate from the G and D modes of amorphous carbon.[28,29] Two additional peaks at 1450 and 1530 cm^{-1} (green fits), which belong to the two characteristic peaks of PMMA at the excitation wavelength of 633 nm,[30] appear after the densification of PMMA by annealing (Figure 4e). Note that these two small peaks also become visible after annealing for graphene lying on the silicon substrate (Supporting Information). The Raman signals of the amorphous carbon increase in intensity with increased PMMA coverage and saturates as the PMMA thickness reaches a few nanometers. This effect is attributed to the so-called graphene-enhanced Raman scattering which has been used to enhance the Raman signals of adsorbed molecules.[31] It is important to note that the Raman signals of the thin amorphous carbon film become discernible only when the graphene is free-standing (Supporting Information). This is presumably due to the stronger graphene-enhanced Raman scattering in the free-standing state. We will leave this issue as the subject of another paper.

To gain a more quantitative view on the Raman intensity of graphene with different degrees of residual PMMA, we consider multiple incident light reflections and interferences in the graphene.[32] Figure 5a,b schematically shows light passing through a single graphene layer and a PMMA/graphene/PMMA sandwich structure, respectively. The electric fields in the various layers are calculated by recurrent transfer matrix formalism for multiple reflections and transmissions with boundary conditions at each interface. The forward (+) and backward (−) amplitudes of the electric field through a stack of N layers can be straightforwardly written as

$$\begin{bmatrix} E_0^- \\ E_0^+ \end{bmatrix} = M \begin{bmatrix} E_N^- \\ E_N^+ \end{bmatrix}$$

with the total transfer matrix M taking the form

$$M = \begin{bmatrix} M_{11} & M_{12} \\ M_{21} & M_{22} \end{bmatrix} \equiv H_{12}L_2 \ldots L_{N-1}H_{N-1,N}$$

H_{ij} and L_j, respectively, represent the interface transition matrix and layer propagation matrix. H_{ij} couples the fields

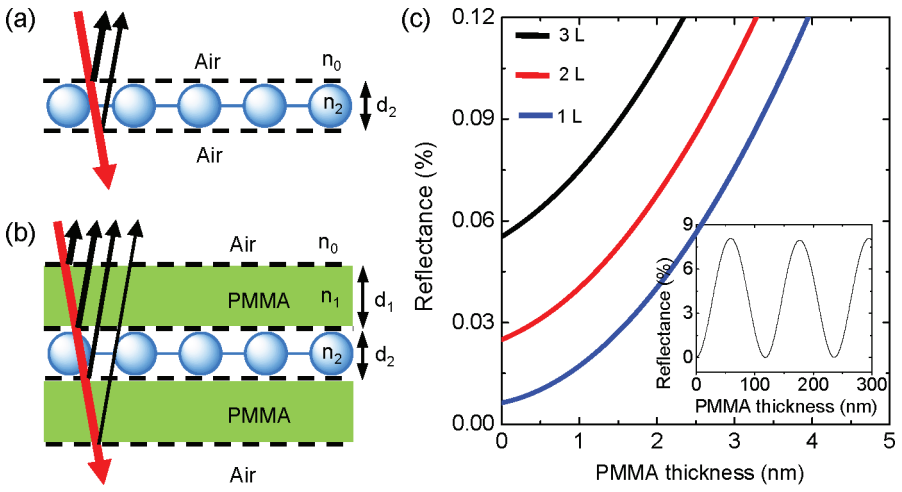

Figure 5. (a) Single graphene layer and (b) PMMA/graphene/PMMA multilayer structure used in the transfer matrix calculation. (c) Calculated reflectance of suspended graphene as a function of PMMA thickness. Up to three graphene layers are shown. The inset displays the same result of a single layer on an extended scale.

on layer i to the fields on layer j by the transmission coefficient t_{ij} and reflection coefficient r_{ij}, whereas L_j counts on the phase shift of the wave in propagating layer j. The two matrices can be expressed as

$$H_{ij} = \frac{1}{t_{ij}}\begin{bmatrix} 1 & r_{ij} \\ r_{ij} & 1 \end{bmatrix} \text{ and } L_j = \begin{bmatrix} e^{-i\alpha_j} & 0 \\ 0 & e^{i\alpha_j} \end{bmatrix}$$

t_{ij} is related to the refractive indices of layer i and j as $2n_i/(n_i + n_j)$, and $r_{ij} = (n_i - n_j)/(n_i + n_j)$. In crossing a given layer from the top to the bottom, a phase factor $e^{-i\alpha}$ is introduced, with an incidence of normal light of $\alpha = 2\pi n_j d_j/\lambda_0$. Simple algebra indicates that the reflectance can be given as $R = |r|^2 = |M_{12}/M_{22}|^2$.

We first consider the case of normal light incidence from air ($n_0 = 1$) onto a suspended single graphene layer which is characterized by a thickness of d_2 (=0.335 nm) and complex refractive index $n_2(\lambda)$ [for $\lambda = 633$ nm, $n_2 \approx 2.0-1.1i$].[33] The imaginary part is responsible for the light adsorption by the graphene. The transfer matrix is simply $M = H_{02}L_2H_{20}$ which, in turn, yields the reflectance $R = [2r_{02} \sin \alpha/(1 - r_{02}^2 e^{-i2\alpha})]^2$. Substituting the n_0, $n_2(\lambda)$, and d_2 into R, we obtain $R \approx 0.0061\%$ of the incident light. This value increases appreciably as d_2 increases (Figure 5c) and can be used to differentiate the number of graphene layers, irrespective of the stacking order of the constituent graphene. Likewise, for a single graphene layer covered on both sides with PMMA, the reflectance can be obtained straightforwardly, using the refractive index of PMMA $n_1 \approx 1.49$, which weakly depends on the wavelength of light. The calculated reflectance oscillates as a function of the thickness of PMMA, as shown in the inset of Figure 5c. This is due to the interference of light in the PMMA/graphene/PMMA sandwich structure. The first maximum intensity occurs at $d_1 = 59$ nm. For $d_1 < 59$, the intensity of the Raman signal increases substantially with the thickness of the PMMA.

Direct assessment of the surface cleanness by Raman scattering is an ingenious method. This can be achieved by using the intensity ratio of the Raman G peak to extract the light reflectance which, in turn, yields the thickness of the contaminant if its refractive index is known. To do this, we revisit the Raman spectra shown in Figure 4d–f for different degrees of surface cleanness. The reflectance is computed *via* the relation $R = (I_G^g/I_G^{g,clean})\beta$, where $I_G^{g,clean}$ is the intensity of the Raman G peak of clean graphene and β is the Raman enhancement factor; β is given as 4.9 and 4.6 for Figure 4d,e, respectively (see Supporting Information for β calculations). Substituting $I_G^g \approx 107$, $I_G^g \approx 61$, and $I_G^{g,clean} \approx 10$, obtained from Figure 4d–f, respectively, into the equation, we obtain $R = 2.19 \pm 0.1\%$ for Figure 4d and $R = 1.31 \pm 0.2\%$ for Figure 4e. Comparing the reflectance shown in Figure 5c yields the thickness of PMMA $d_1 = 2.4 \pm 0.2$ nm for Figure 4d and $d_1 = 0.9 \pm 0.5$ nm for Figure 4e. This result indicates that only the PMMA submonolayer is covered on partially clean graphene, in good agreement with the TEM image shown in Figure 4b. For the complete coverage of PMMA (Figure 4a), our calculated thickness is also consistent with the value (~2.0 nm) reported by the measurements of scanning electron microscopy.[22]

CONCLUSION

In summary, we have demonstrated the clean transfer of graphene using polycarbonate, free of contaminants such as residual PMMA that typically remain in the conventional transfer process. Combining TEM and Raman measurements, we show that the Raman spectra of graphene with various degrees of surface cleanness exhibit rather distinctive features that can be used to qualitatively assess the surface cleanness of suspended graphene. A model based on multiple light reflections and interferences between the graphene and contaminant layers is also developed to quantitatively

estimate the thickness of the contaminants on the graphene. The technique presented here opens up a new means of obtaining graphene with a high-quality surface and directly impacts its applications on surface chemistry, biotechnology, and high-mobility electronics.

METHODS

Graphene Growth. Graphene sheets used in the current study were grown by atmospheric pressure CVD of methane (99.99%) on polycrystalline Cu foils. Prior to growth, the Cu foils were cleaned by acetic acid to remove surface oxides. Then, the Cu foils were mounted in the CVD chamber with a steady 10 sccm flow of hydrogen. The furnace was ramped up to 1000 °C over 40 min. In the CVD process, methane (20 sccm) mixed with argon (230 sccm) and hydrogen (10 sccm) was fed into the reaction chamber for 2 min during which graphene growth occurs. The Cu foils were then moved to the cooling zone where a cooling system is equipped.

TEM Characterizations. A JEOL 2100F transmission electron microscope equipped with the DELTA correctors (including an imaging aberration corrector) was operated at 60 kV.[34] The specimens were kept at an ambient temperature during the observation. The TEM images were recorded by a Gatan CCD (model 894) with the typical exposure time of 1−2 s.

Raman Characterizations. Micro-Raman spectra were obtained on CVD graphene in a commercial Raman microscope (HR800, HORIBA). The measurements were performed at room temperature with laser excitation wavelength of 633 nm. A 100× objective was used to provide a diffraction-limited spot size of about 1 μm. A low power level (<1 mW) is taken to avoid any heating effect. Lorentzian fits were used throughout the Raman spectra presented in Figure 4 and in Figures S3 and S4 (Supporting Information).

Acknowledgment. C.J. and K.S. acknowledge the supports from JST-CREST and Grant-in-Aid for Scientific Research from MEXT (#19054017). The other authors also acknowledge the support of the NTHU booster project and TSMC JDP project under Contract No. NTHU0905, and of the Taiwan National Science Council under Contract No. NSC 97-2112-M-007-016-MY3.

Supporting Information Available: Additional Raman spectra of graphene covered with a thin layer of PMMA and Raman spectra of amorphous carbon on suspended graphene are given in Figures S1 and S2. Calculations of Raman enhancement factors are given in Figure S3 and S4. This material is available free of charge *via* the Internet at http://pubs.acs.org.

REFERENCES AND NOTES

1. Geim, A. K.; Novoselov, K. S. The Rise of Graphene. *Nat. Mater.* **2007,** *6*, 183–191.
2. Schedin, F.; Geim, A. K.; Morozov, S. V.; Hill, E. W.; Blake, P.; Katsnelson, M. I.; Novoselov, K. S. Detection of Individual Gas Molecules Adsorbed on Graphene. *Nat. Mater.* **2007,** *6*, 652–655.
3. Meyer, J. C.; Girit, C. O.; Crommie, M. F.; Zettl, A. Imaging and Dynamics of Light Atoms and Molecules on Graphene. *Nature* **2008,** *454*, 319–322.
4. Wilson, N. R.; Pandey, P. A.; Beanland, R.; Young, R. J.; Kinloch, I. A.; Gong, L.; Liu, Z.; Suenaga, K.; Rourke, J. P.; York, S. J.; Sloan, J. Graphene Oxide: Structural Analysis and Application as a Highly Transparent Support for Electron Microscopy. *ACS Nano* **2009,** *3*, 2547–2556.
5. Sloan, J.; Liu, Z.; Suenaga, Kazu.; Wilson, N. R.; Pandey, P. A.; Perkins, L. M.; Rourke, J. P.; Shannon, I. J. Imaging the Structure, Symmetry, and Surface-Inhibited Rotation of Polyoxometalate Ions on Graphene Oxide. *Nano Lett.* **2010,** *10*, 4600–4606.
6. Wanunu, M.; Dadosh, T.; Ray, V.; Jin, J.; McReynolds, L.; Drndic, M. Rapid Electronic Detection of Probe-Specific MicroRNAs Using Thin Nanopore Sensors. *Nat. Nanotechnol.* **2010,** *5*, 807–814.
7. Sun, X.; Liu, Z.; Welsher, K.; Robinson, J. T.; Goodwin, A.; Zaric, S.; Dai, H. Nano-Graphene Oxide for Cellular Imaging and Drug Delivery. *Nano Res.* **2008,** *1*, 203–212.
8. Coletti, C.; Riedl, C.; Lee, D. S.; Krauss, B.; Patthey, L.; von Klitzing, K.; Smet, J. H.; Starke, U. Charge Neutrality and Band-Gap Tuning of Epitaxial Graphene on SiC by Molecular Doping. *Phys. Rev. B* **2010,** *81*, 235401.
9. Lin, Y. C.; Lin, C. Y.; Chiu, P. W. Controllable Graphene N-Doping with Ammonia Plasma. *Appl. Phys. Lett.* **2010,** *96*, 133110.
10. Li, X.; Zhu, Y.; Cai, W.; Borysiak, M.; Han, B.; Chen, D.; Piner, R. D.; Colombo, L.; Ruoff, R. S. Transfer of Large-Area Graphene Films for High-Performance Transparent Conductive Electrodes. *Nano Lett.* **2009,** *9*, 4359–4363.
11. Alman, B.; Regan, W.; Aloni, S.; Altoe, V.; Alem, N.; Girit, C.; Geng, B.; Maserati, L.; Crommie, M.; Wang, F.;*et al.*Transfer-Free Batch Fabrication of Large-Area Suspended Graphene Membranes. *ACS Nano* **2010,** *4*, 4762–4768.
12. Park, H. J.; Meyer, J.; Roth, S.; Skakalova, V. Growth and Properties of Graphene Prepared by Chemical Vapor Deposition. *Carbon* **2010,** *48*, 1088–1094.
13. Li, X.; Cai, W.; An, J.; Kim, S.; Nah, J.; Yang, D.; Piner, R.; Velamakanni, A.; Jung, I.; Tutuc, E.; Banerjee, S. K.; Colombo, L.; Ruoff, R. S. Large-Area Synthesis of High-Quality and Uniform Graphene Films on Copper Foils. *Science* **2009,** *324*, 1312–1314.
14. Ferrari, A. C. Raman Spectroscopy of Graphene and Graphite: Disorder, Electron−Phonon Coupling, Doping and Nonadiabatic Effects. *Solid State Commun.* **2007,** *143*, 47–57.
15. Pimenta, M. A.; Dresselhaus, G.; Dresselhaus, M. S.; Cançado, L. G.; Jorio, A.; Saito, R. Studying Disorder in Graphite-Based Systems by Raman Spectroscopy. *Phys. Chem. Chem. Phys.* **2007,** *9*, 1276–1291.
16. Pisana, S.; Lazzeri, M.; Casiraghi, C.; Novoselov, K. S.; Geim, A. K.; Ferrari, A. C.; Mauri, F. Breakdown of The Adiabatic Born−Oppenheimer Approximation in Graphene. *Nat. Mater.* **2007,** *6*, 198–201.
17. Das, A.; Pisana, S.; Chakraborty, B.; Piscanec, S.; Saha, S. K.; Waghmare, U. V.; Novoselov, K. S.; Krishnamurthy, H. R.; Geim, A. K.; Ferrari, A. C.; Sood, A. K. Monitoring Dopants by Raman Scattering in an Electrochemically Top-Gated Graphene Transistor. *Nat. Nanotechnol.* **2008,** *3*, 210–215.
18. Yan, J.; Zhang, Y.; Kim, P.; Pinczuk, A. Electric Field Effect Tuning of Electron−Phonon Coupling in Graphene. *Phys. Rev. Lett.* **2007,** *98*, 166802.
19. Lazzeri, M.; Piscanec, S.; Mauri, F.; Ferrari, A. C.; Robertson, J. Phonon Linewidths and Electron−Phonon Coupling in Graphite and Nanotubes. *Phys. Rev. B* **2006,** *73*, 155426.
20. Giovannetti, G.; Khomyakov, P. A.; Brocks, G.; Karpan, V. M.; van den Brink, J.; Kelly, P. J. Doping Graphene with Metal Contacts. *Phys. Rev. Lett.* **2008,** *101*, 026803.
21. Saito, R.; Jorio, A.; Souza Filho, A. G.; Dresselhaus, G.; Dresselhaus, M. S.; Pimenta, M. A. Probing Phonon Dispersion Relations of Graphite by Double Resonance Raman Scattering. *Phys. Rev. Lett.* **2002,** *88*, 027401.
22. Geringer, V.; Subramaniam, D.; Michel, A. K.; Szafranek, B.; Schall, D.; Georgi, A.; Mashoff, T.; Neumaier, D.; Liebmann, M.; Morgenstern, M. Electrical Transport and Low-Temperature Scanning Tunneling Microscopy of Microsoldered Graphene. *Appl. Phys. Lett.* **2010,** *96*, 082114.

23. Booth, T. J.; Blake, P.; Nair, R. R.; Jiang, D.; Hill, E. W.; Bangert, U.; Bleloch, A.; Gass, M.; Novoselov, K. S.; Katsnelson, M. I.; Geim, A. K. Macroscopic Graphene Membranes and Their Extraordinary Stiffness. *Nano Lett.* **2008,** *8*, 2442–2446.
24. Blake, P.; Hill, E. W.; Castro Neto, A. H.; Novoselov, K. S.; Jiang, D.; Yang, R.; Booth, T. J.; Geim, A. K. Making Graphene Visible. *Appl. Phys. Lett.* **2007,** *91*, 063124.
25. Casiraghi, C.; Hartschuh, A.; Lidorikis, E.; Qian, H.; Harutyunyan, H.; Gokus, T.; Novoselov, K. S.; Ferrari, A. C. Rayleigh Imaging of Graphene and Graphene Layers. *Nano Lett.* **2007,** *7*, 2711–2717.
26. Roddaro, S.; Pingue, P.; Piazza, V.; Pellegrini, V.; Beltram, F. The Optical Visibility of Graphene: Interference Colors of Ultrathin Graphite on SiO_2. *Nano Lett.* **2007,** *7*, 2707–2710.
27. Wang, Y. Y.; Ni, Z. H.; Shen, Z. X.; Wang, H. M.; Wu, Y. H. Interference Enhancement of Raman Signal of Graphene. *Appl. Phys. Lett.* **2008,** *92*, 043121.
28. Ferrari, A. C.; Robertson, J. Raman Spectroscopy of Amorphous, Nanostructured, Diamond-like Carbon, and Nanodiamond. *Philos. Trans. R. Soc. London, Ser. A* **2004,** *362*, 2477–2512.
29. Capano, M. A.; McDevitt, N. T.; Singh, R. K.; Qian, F. Characterization of Amorphous Carbon Thin Films. *J. Vac. Sci. Technol., A* **1996,** *14*, 431–435.
30. Thomas, K. J.; Sheeba, M.; Nampoori, V. P. N.; Vallabhan, C. P. G.; Radhakrishnan, P. Raman Spectra of Polymethyl Methacrylate Optical Fibres Excited by a 532 nm Diode Pumped Solid State Laser. *J. Opt. A: Pure Appl. Opt.* **2008,** *10*, 055303.
31. Ling, X.; Xie, L.; Fang, Y.; Xu, H.; Zhang, H.; Kong, J.; Dresselhaus, M. S.; Zhang, J.; Liu, Z. Can Graphene Be Used as a Substrate for Raman Enhancement?. *Nano Lett.* **2010,** *10*, 553–561.
32. Klein, M. V.; Furtak, T. E. *Optics*; Wiley: New York, 1986.
33. Ni, Z. H.; Wang, H. M.; Kasim, J.; Fan, H. M.; Yu, T.; Wu, Y. H.; Feng, Y. P.; Shen, Z. X. Graphene Thickness Determination Using Reflection and Contrast Spectroscopy. *Nano Lett.* **2007,** *7*, 2758–2763.
34. Sasaki, T.; Sawada, H.; Hosokawa, F.; Kohno, Y.; Tomita, T.; Kaneyama, T.; Kondo, Y.; Kimoto, K.; Sata, Y.; Suenaga, K. Performance of Low-Voltage STEM/TEM with Delta Corrector and Cold Field Emission Gun. *J. Electron Microsc.* **2010,** *59*, S7–S13.